ELSEVIER

Journal of Nuclear Materials 296 (2001) 183–191

journal of nuclear materials

www.elsevier.com/locate/jnucmat

Origin of hardening and deformation mechanisms in irradiated 316 LN austenitic stainless steel

E.H. Lee, T.S. Byun, J.D. Hunn *, K. Farrell, L.K. Mansur

Oak Ridge National Laboratory, Metals and Ceramics Division, P.O. Box 2008, Bldg. 4500s, MS-6151, Oak Ridge, TN 37831-6151, USA

Abstract

The effects of displacement damage and trapped helium on deformation microstructures in AISI 316 LN austenitic stainless steel were studied by applying a newly developed disk bend method to specimens irradiated with 360 keV He ions at 200°C. Radiation damage microstructures consisted of an intimate mix of black dots, dislocation loops, and very small helium filled cavities. In the unirradiated specimens, the deformation mode upon straining was planar glide with cross-slip. With increasing dose, cross-slip was progressively restricted. Correspondingly, deformation microstructure changed from dislocation network dominant to channeling dominant. The channel bands were composed of piled-up dislocations, stacking faults, and twinned layers. Published by Elsevier Science B.V.

1. Introduction

Hardening by helium, and associated degradation of mechanical properties, is one of the concerns for the austenitic stainless steel to be used as the containment shroud of the mercury target in the US Spallation Neutron Source. In particular, our recent work showed that He-induced hardening could exceed that produced by Fe-induced displacement damage at high helium levels (>1 at.%) [1]. Although such a high level of helium accumulation is not expected during the service lifetime of the target, it is still of genuine interest in understanding the potential impact of helium on mechanical properties.

Even though the deformation of irradiated metals has been studied since the 1960s [2–14], the nature of deformation microstructures is not yet well understood. In general, deformation microstructures of irradiated and deformed austenitic steels have been characterized by piled-up dislocations, stacking faults, twin bands, and defect-reduced channels [8–16]. However, the relative preponderance of these defects was thought to vary with test temperature and/or strain rate. It was reported for 5 MeV Ni-ion irradiated 304L austenitic stainless steel that twinning was a dominant deformation mode at low temperature (25°C) and/or moderate strain rate (10^{-4}), whereas dislocation channeling became prominent at higher temperature (>288°C) and/or lower strain rate (10^{-6}) [10–12]. A similar observation was made for 304L austenitic stainless steel neutron irradiated at 277°C, in that twinning was dominant at room temperature testing and defect-reduced channeling at 277°C testing [15]. On the other hand, in other studies, twinning was found at a test temperature as high as 450°C for 304 austenitic stainless steel irradiated by neutrons [8] and at 330°C for J316 austenitic stainless steel irradiated by neutrons [16]. In the former work [8], a uniaxial tensile test at above 600°C produced homogeneously distributed network dislocations, indicating that cross-slip and thermally activated processes were dominant deformation modes at elevated temperatures. In the latter work [16], dislocation channeling was also observed in 330°C tests. Summarizing this information, one could conclude that there exists an upper temperature limit above which planar glide is no longer sustained due to thermally activated processes, but both twinning and channeling are operating below that temperature. In fact, the view that twin or channel formation is dependent on test temperature and/or strain rate

* Corresponding author. Tel.: +1-865 574 2480; fax: +1-865 574 0641.

E-mail address: hunnjd@ornl.gov (J.D. Hunn).

0022-3115/01/$ - see front matter. Published by Elsevier Science B.V.
PII: S0022-3115(01)00566-9

can be misleading. In our recent work on stainless steel, we found that the same deformation bands could be imaged by transmission electron microscopy (TEM) as either piled-up dislocations, twins, stacking faults, or defect-reduced channels, simply by varying the imaging condition [17,18]. It was demonstrated that all these deformation microstructures were different manifestations of the same glide dislocations, which were separated into Shockley partials.

With this new insight, deformation microstructures of AISI 316 LN austenitic stainless steel were studied after irradiation with 360 keV He-ions to various doses. Tests were also conducted for specimens irradiated with 3500 keV Fe-ions only (without helium) to investigate the role of helium on deformation. Deformation microstructures were produced by a recently developed disk-bend method [19,20], and microstructural analyses were conducted by TEM.

2. Experimental

The material used for this experiment was an AISI 316 LN stainless steel acquired from Jessop Steel Company (Heat #18474). The steel was solution annealed in vacuum for 30 min at 1050°C before irradiation. The nominal composition of the alloy was, in weight percent, 16.3 Cr, 10.2 Ni, 2.01 Mo, 1.75 Mn, 0.39 Si, 0.009 C, 0.11 N, 0.029 P with the balance Fe. The specimens were in the form of 3 mm diameter disks, 0.25 mm thick, which were polished first mechanically and subsequently electrochemically prior to irradiation. For this study, specimens were irradiated at 200°C with 360 keV He^+ or 3500 keV Fe^+ ions using 2.5 and 5 MV Van de Graaff accelerators. These ion energies produced maximum helium deposition and displacement damage at a depth of 750–850 nm according to calculations by the computer code, Stopping and Range of Ions in Matter (SRIM, 2000 version) [21]. The procedure for the dpa calculation is described in [22,23].

Helium was deposited at a rate of 0.02 to 2 appm/s at the peak, producing displacement damage at a rate of 2×10^{-6} to 2×10^{-4} dpa/s. Specimens were prepared with helium concentration ranging from 2 appm (2×10^{-4} at.%) to 200 000 appm (20 at.%). The corresponding displacement doses were from 10^{-4} to ~15 dpa. Irradiation was also carried out with 3500 keV Fe^+ ions to 10 dpa at a rate of 2 to 3×10^{16} ions/m^2/s ($\sim 1 \times 10^{-3}$ dpa/s at the peak).

After irradiation, the specimens were deformed at room temperature by bending them around the surface of a 1 mm diameter tungsten carbide ball, which was placed on the unirradiated side of the disks. About 10% plastic strain was introduced at the irradiated surface for all disk-bend tested specimens. In the deformation fixture, the disks were clamped at the rim between two mating screws with a center bore to accommodate the ball and a push rod. A load of up to 30 N was applied to the push rod with a Tinius Olsen testing machine, deforming the disk at a strain rate of approximately 10^{-2} per second. The displacements of the machine crosshead and the deflection of the bottom of the disk, measured by a linear variable differential transducer (LVDT), were recorded during deformation. The plastic thickness change was calculated after removing the load, to eliminate the elastic component in specimen and fixture. The surface strain of the irradiated side (ε_S^P) was determined by the relation

$$\varepsilon_S^P = 2\varepsilon_Z^P - \varepsilon_I^P, \tag{1}$$

where ε_Z^P is the average strain at the middle of the disk, determined by the relation

$$\varepsilon_Z^P = \ln(t_0/t), \tag{2}$$

with t_0 and t being the thickness of the center region of the disk before and after deformation, respectively. The ball contact surface plastic strain (ε_I^P) was determined by the empirical formula

$$\varepsilon_I^P = 0.2(d_p/D), \tag{3}$$

derived by Tabor [24], where d_p was the optically determined indentation (plastic) diameter and D was the ball diameter. Detailed procedure for this method and analysis can be found in [19,20,25]. Eq. (1) assumes a linear strain gradient through the thickness of the disk. This assumption could be somewhat affected by the discontinuity in hardness between the unirradiated bulk and the irradiation hardened surface layer. However, cross-sectional TEM shows no indication of catastrophic discontinuity in the applied strain at the interface between the bulk and irradiated layer, as would be evidenced by cracking or heavy dislocation pile-up.

After deformation, an ~700 nm thick surface layer was removed electrochemically from the irradiated side of the disks to expose the peak radiation damage region. The specimens were then thinned from the unirradiated side until perforation. In this way, ~100 nm thick TEM foils were prepared for examination of the deformation microstructure at an original depth between 700 and 800 nm. A philips CM12 electron microscope was used at 120 keV operating voltage for examination of the deformed microstructure.

3. Results

Before deformation, the microstructures of the as-irradiated specimens consisted of small black dots (vacancy and interstitial clusters), small faulted Frank interstitial loops (Burgers vectors $\mathbf{b} = a/3\langle 1\,1\,1\rangle$), some unfaulted loops ($\mathbf{b} = a/2\langle 1\,1\,0\rangle$), where a is the unit

lattice parameter, and small helium bubbles. Helium bubbles were too small to be seen at low doses (<1 at.% He). Above 1 at.% He, discernible bubble features began to appear. Although a precise measurement was not possible at low doses, both defect cluster number density and size increased with dose and saturated around 5 at.%. Above 20 at.% He, blistering and exfoliation occurred. Detailed irradiation microstructures were reported in a previous paper [26]. This paper describes post-deformation microstructures for a set of specimens irradiated in parallel with those prepared for that investigation of radiation-induced microstructures.

As an aid to understanding the deformation microstructures, recall that austenitic stainless steel has a face-centered-cubic crystallographic arrangement of atoms and a favored slip system of $\langle 1\,1\,0\rangle\{1\,1\,1\}$.The fcc structure consists of close packed $\{1\,1\,1\}$ layers with a stacking sequence ...ABCABC..., where each atom in a given $\{1\,1\,1\}$ layer rests in the 'valley' between three atoms in the adjacent $\{1\,1\,1\}$ layer. As a dislocation glides along a $\{1\,1\,1\}$ plane, the atoms on one side of the glide plane move by one Burgers vector relative to the atoms on the other side; traveling to the next valley in that direction as the dislocation passes through. A Burgers vector of $\mathbf{b} = a/2\langle 1\,1\,0\rangle$ represents the minimum dislocation glide that preserves the stacking order. However, a dislocation motion of $a/2\langle 1\,1\,0\rangle$ may be achieved at lower energy by zigzagging in two $\langle 2\,1\,1\rangle$ directions. Thus, a perfect $\langle 1\,1\,0\rangle$ dislocation splits into two Shockley partial dislocations (e.g., $a/2[1\,1\,0] = a/6[1\,2\,1] + a/6[2\,1\,\bar{1}]$). These partial dislocations can move independently. If a leading partial is gliding along a $\{1\,1\,1\}$ A-layer, as the partial move through, the atoms on the other side of the glide plane shift with respect to the A-layer by a Burgers vector $\mathbf{b} = a/6\langle 2\,1\,1\rangle$, leaving behind a faulted stacking sequence of ...ABCA**CABC**... The trailing partial restores the normal stacking order as it passes through, with a net slip of each atom above the glide plane of $a/2$ in the $\langle 1\,1\,0\rangle$ direction.

In simple systems, the separation between the leading and trailing partials (i.e., the width of the stacking fault) depends on the stacking fault energy. Many fcc metals, such as copper and aluminum, have high stacking fault energies, so the separation of the Shockley partials is very small and not usually obvious in TEM except by using careful weak-beam techniques [27,28]. In contrast, stainless steel has a relatively low stacking fault energy, giving rise to greater, more visible separation of the partials. The width of these stacking faults can also be affected by lattice defects, which can act to impede glide of one or both of the partials. The presence of a stacking fault limits cross-slip, because the fault must first be forcibly constricted to restore the perfect dislocation before cross-slip can occur. Thus, low stacking fault energy is one reason why slip in stainless steel is more planar than in copper or aluminum. Another explanation may be the occurrence of short-range order in the stainless steel [29].

In fcc crystals, the close-packed $\{1\,1\,1\}$ glide planes are also the coherent twin planes, and the stacking faults that form between Shockley partials can be directly related to twin formation [17,18]. Consider the intrinsic (missing B-layer) stacking fault created by the glide of a leading partial on a $\{1\,1\,1\}$ A-plane, ...ABC**A**<u>**C**</u>**ABC**..., as described above. The layers <u>A</u> and <u>C</u> form two mirror planes for what can be considered as two 'one-layer prototwins' (i.e., C<u>A</u>C and A<u>C</u>A). Although these do not satisfy the classic definition of a twin, in that they do not extend over at least one full lattice parameter, they are precursors of that condition and will produce twin streaks in electron diffraction patterns. If a second leading partial dislocation were to glide through on the new C-layer, prior to the trailing partial associated with the first leading partial moving through on the A-layer to restore the stacking sequence, then an extrinsic (extra C-layer) stacking fault ...ABC<u>A</u>C**B**<u>**C**</u>**A**... would result. Here the mirror planes <u>A</u> and <u>B</u> have moved apart to produce two 'two-layer prototwins' (i.e., BC<u>A</u>CB and AC<u>B</u>CA). This process can continue with successive overlapping glide of leading partials, resulting in a structure that meets the classic definition of a twin. Because this twinning mechanism relies on the overlapping of Shockley partials on successive $\{1\,1\,1\}$ planes, it becomes more evident under conditions that force dislocations to glide in narrower bands.

Both unirradiated and irradiated specimens were deformed by up to 10% strain at room temperature using the disk-bend method. Deformed microstructures consisted of a varying degree of network dislocations and planar dislocation arrays, depending upon the magnitude of the radiation dose. Fig. 1 shows glide dislocations for the specimens irradiated to 20, 200 and 10 000 appm helium and strained to 10%. In the figure, the appearance of bounded stacking fault fringes indicates that glide dislocations separated into Shockley partials. The separation of Shockley partials became increasingly conspicuous with increasing dose (i.e., increasing concentration of radiation-induced defects such as helium clusters, black dots, and Frank loops).

Fig. 2 illustrates the deformation microstructures of unirradiated and irradiated specimens with helium levels from 20 appm (0.0015 dpa) to 20 at.% (15 dpa). Unirradiated or low dose irradiated microstructures were characterized by random network dislocations, indicating that cross-slip occurred in the absence, or for a low concentration, of radiation-induced defects. At 200 appm He, cross-slip was severely restricted and dislocation glide was mostly planar. At 2000 appm He, patches of stacking fault fringes became conspicuous on the glide planes, indicating that some glide dislocations were quite widely separated into Shockley partials. With

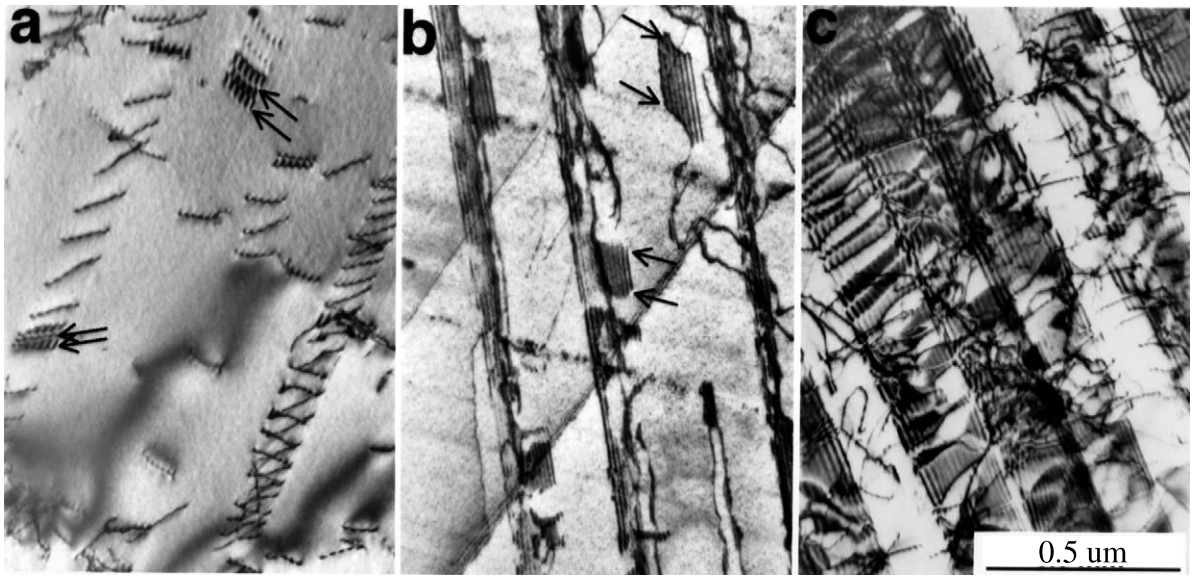

Fig. 1. Glide dislocation microstructure of 316 LN austenitic stainless steel irradiated at 200°C with 360 keV He-ions to (a) 20 appm, (b) 2000 appm, and (c) 10 000 appm helium, and strained to 10% at room temperature by the disk-bend method. Stacking fault fringes are bounded by two pairing partials as marked by the arrows.

increasing helium dose, the propensity for separated partials increased and the faulted regions on adjacent glide planes began to overlap forming complex twin bands. Beyond 2 at.% He, very little cross-slip occurred and very few dislocations were found in the matrix between twin bands. An important observation was that, at low doses, deformation occurred uniformly throughout the grain due to frequent cross-slip of dislocations. With increasing dose, deformation was progressively localized and cross-slip was discouraged.

During deformation, radiation-induced Frank interstitial loops that were intersected by slip bands became unfaulted, assisted by the stress field of piled-up dislocations in the bands, and were subsequently mostly cleared out of the deformation band, presumably by prismatic glide. This reduction of radiation defects within the bands was best seen when the twin bands or the stacking fault fringe bands were imaged edge-on. This is an imaging condition at which the $\{1\,1\,1\}$ glide planes containing the twin bands are parallel to the beam direction and the images of dislocations on those planes becomes weak or out of contrast because of the satisfied $\mathbf{g}\cdot\mathbf{b}=0$ condition and because the defects adjacent to the band do not overlap with the channel band. Here, it should be pointed out that Frank loops are not removed by successive slicing of loops by glide dislocations, as has been suggested in the past [14,30]. Slicing a loop produces jogs on the loop and makes it more difficult to move [9,18]. For this reason, there were always some persistent Frank loops remaining in the channel bands. Thus, a terminology 'defect-reduced channel band' is used here instead of 'defect-free channel band'.

As mentioned earlier, in the unirradiated condition, deformation induced dislocations were distributed homogeneously and no banding occurred at 10% strain level. It should be pointed out that channeling does occur in unirradiated materials at high strain level once dislocation networks are fully developed [17]. Fig. 3 illustrates defect-reduced channel bands for the helium concentration range from 0.2 at.% (0.15 dpa) to 20 at.% (15 dpa). These channel bands are the deformation stacking fault/twin bands viewed exactly edge-on. In this mode they appear to be similar to the defect-free channels found in many strained metals after irradiation or prior plastic deformation. At 0.2 at.% He, narrow channel bands and some random glide dislocations were developed. With increasing dose, cross-slip was suppressed, progressively resulting in reduced network dislocations and increased channeling. Noteworthy features of the channel bands were their narrow thicknesses and the short distances between them when compared with dislocation channels observed in other irradiated fcc metals. For example, in neutron-irradiated copper [31,32] and gold [33] strained at room temperature, the channel widths are typically about 0.1 μm and have spacings of 1 to 3 μm. In copper, these values are decreased by factors of only 2 or so by increases in fast neutron fluence over a range of three orders of magnitude to 8×10^{24} n/m^2 ($\sim$1.5 dpa), and by testing the higher fluence specimens at a reduced temperature of 4 K. Testing at cryogenic temperature might be con-

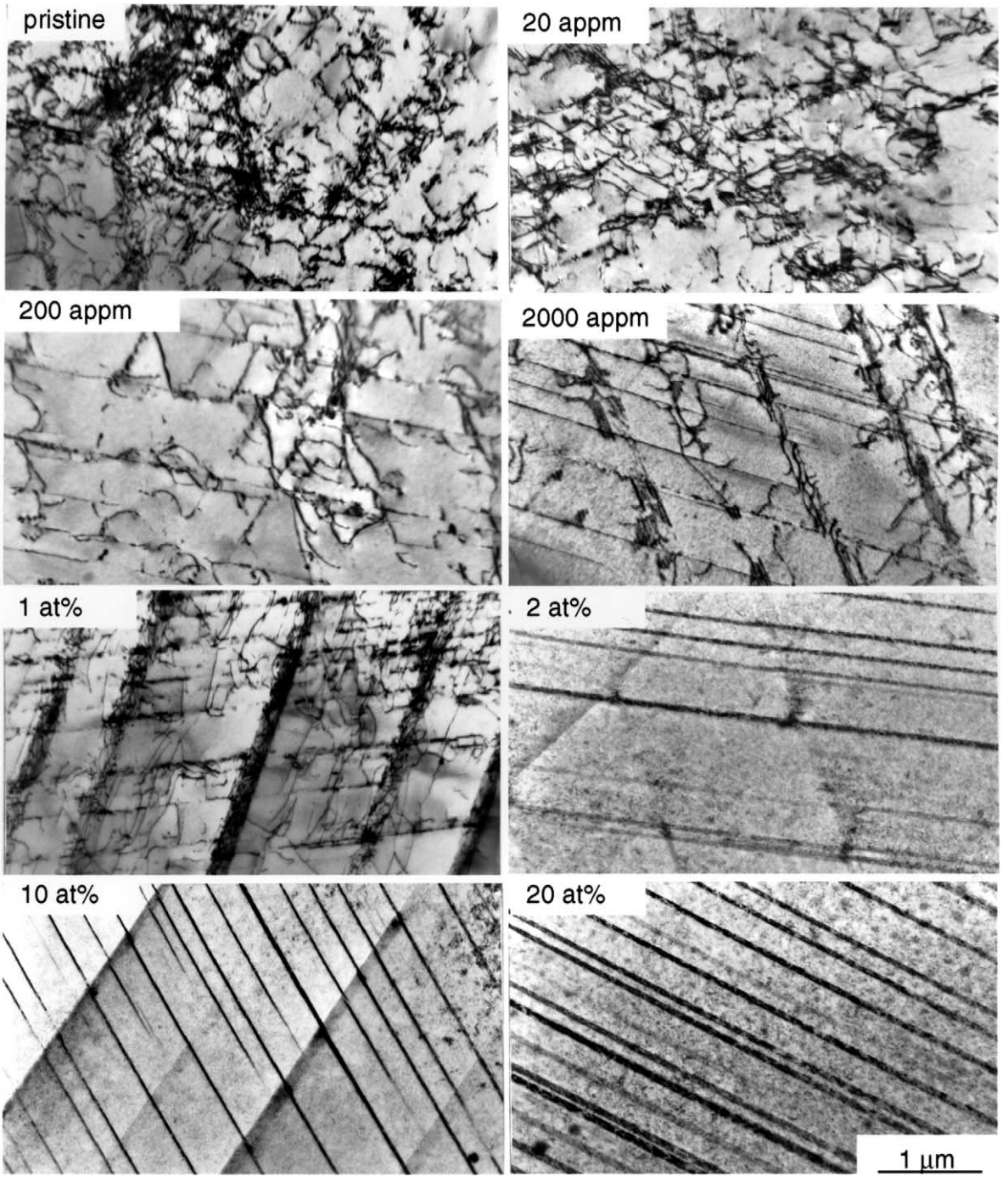

Fig. 2. Deformation microstructure for 316 LN austenitic stainless steel irradiated at 200°C with 360 keV He ions to various helium levels and strained to 10% at room temperature by the disk-bend method.

sidered the equivalent of testing at higher doses. These conditions are representative of copper irradiated to displacement damage levels that overlap those in the present work and are therefore appropriate for comparison. In the present work, the channel widths and spacings are each a factor of 10 smaller than those observed in copper. While there was considerable grain-to-grain variation in channel characteristics, which made

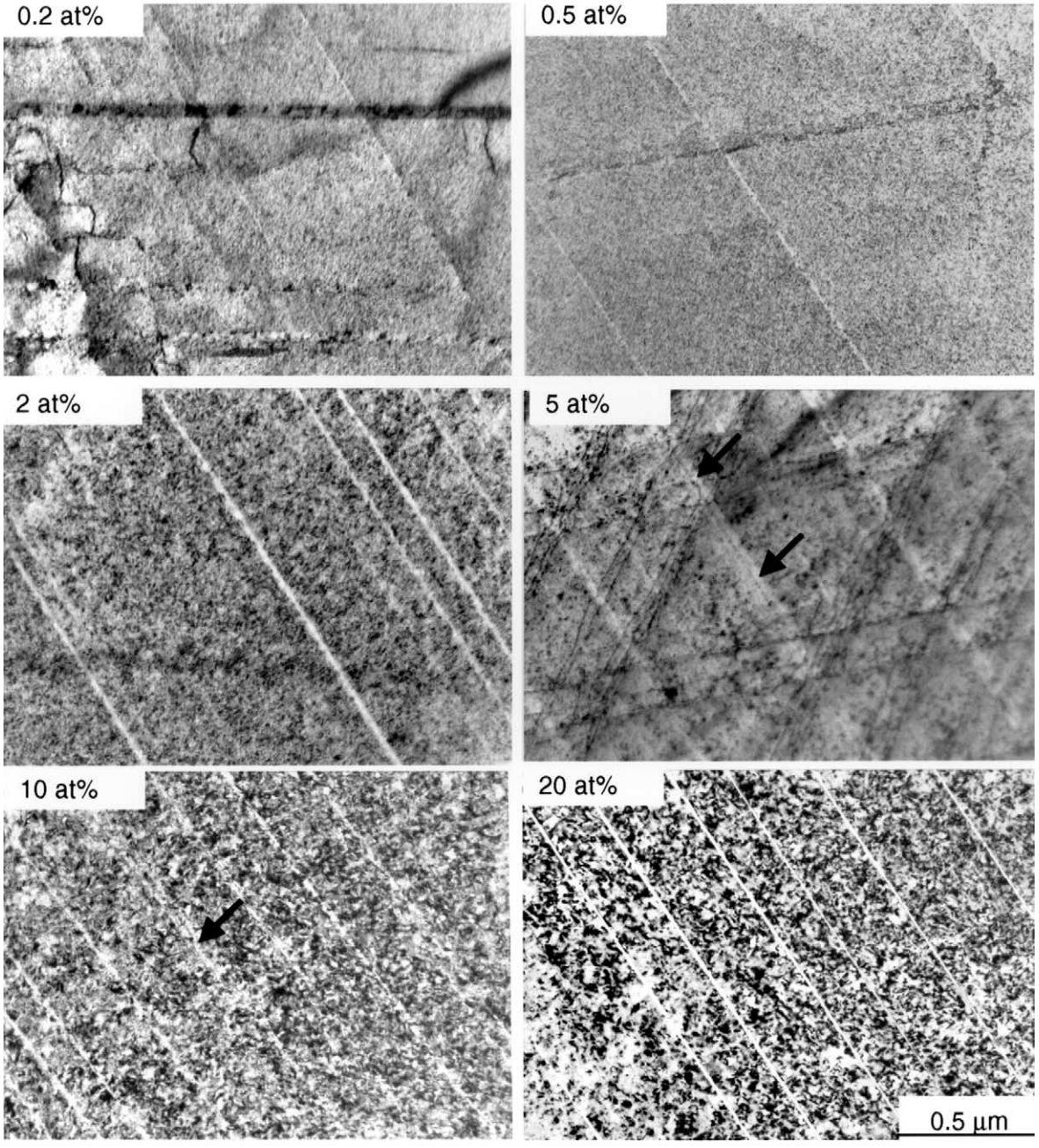

Fig. 3. Dose dependence of channel band formation for 316 LN austenitic stainless steel irradiated at 200°C with 360 keV He ions to various helium levels and strained to 10% at room temperature by the disk-bend method.

precise measurements of the channels widths and frequencies impossible, there was no doubt about the small sizes (Fig. 3). From rough measurements we found that the channel width (thickness when viewed edge on) averaged about 7 nm at the lower doses of 0.2–0.5% He, to about 10 nm at 10–20% He. At intermediate doses of 2–5%, the average width was about 12 nm but the spread of widths was larger, up to 70 nm. Many of the larger channels contained discontinuous center strips of unidentified microstructure. These strips suggest that the wider channels were a result of the merger of adjacent channel bands. The band spacing was of the order of 350 nm for the lower doses, 200 nm for intermediate doses, and about 250 nm for the higher doses. The order of

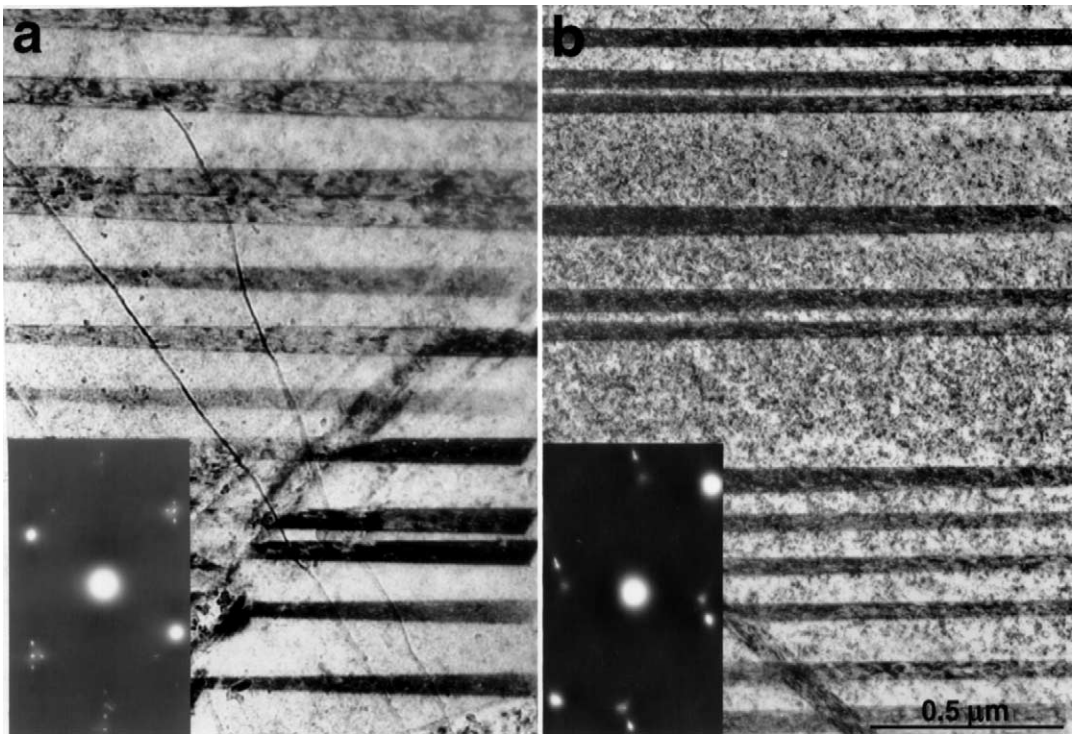

Fig. 4. Deformation microstructures strained to 10% at room temperature by the disk-bend method for 316 LN irradiated at 200°C to (a) 10 dpa with 3500 keV Fe and (b) 1.5 dpa (2 at.% He) with 360 keV He.

magnitude difference in channel width and spacing, compared to irradiated copper, is too large to be due to differences in dose alone. They must be caused by inherent differences in deformation behavior between copper and stainless steel.

An important observation in helium irradiated stainless steel was that helium bubbles still remained in the channel bands although a significant fraction of Frank loops were cleared. In our recent work, a dramatic increase in hardness was observed in association with bubble formation when helium was implanted beyond 1 at.% [1]. In an effort to understand the excessive hardening by helium, deformation microstructure was examined for a specimen irradiated to 10 dpa at 200°C with 3500 keV Fe ions and strained to 10% at room temperature by the disk-bend method. Fig. 4 compares the deformation microstructures of 10 dpa Fe-ion irradiated and 1.5 dpa (2 at.% He) He-ion irradiated specimens. The extent of twin band microstructures were very similar for both specimens, even though displacement damage by helium was several times lower, indicating that helium bubbles had augmented the hardening. However, the deformation microstructures were still the same type whether helium was present or not. Deformation mode was not changed by the presence of helium. The only observable difference was that cross-slip was restricted at a lower displacement damage level in the presence of helium.

4. Discussion

In the absence of radiation-induced defects, cross-slip and tangling of dislocations occurred frequently. Therefore, a blocky dislocation network characterized the deformation microstructure of the unirradiated specimen. With increasing helium and radiation-induced defects (black dots and dislocation loops), cross-slip was progressively suppressed because of the widening of stacking faults. Both helium clusters and radiation-induced defects have been found to restrict dislocation motion [34].

Glide dislocations separated into more easily observable Shockley partials with increasing dose. Such a trend was observed at a dose as low as 20 appm He (0.0015 dpa), as black dots or small Frank interstitial loops began to form. Analyses [17,18] revealed that a direct interaction of a Frank loop with a leading Shockley partial produces jogs and stair-rod partials on the loop which in turn impede the motion of the trailing partial by jog-pinning and stair-rod locking, enhancing the spatial separation of the Shockley partials.

As the concentration of defect clusters increases, the spacing between dislocation barriers decreases and the critical stress required for breakaway increases, although it does not increase without bound. This increases the yield strength, as observed in neutron irradiated 316 SS [35] and 800 MeV proton-irradiated 304L SS [36]. The dislocation is nominally straight under such conditions and cross-slip is restricted. Deformation is concentrated within narrow channel bands, resulting in reduced elongation. In particular, during deformation, the number density of Frank loops is reduced in the channel bands and most dislocation glide occurs in these bands. Thus, in a highly defected microstructure, most deformation is localized in bands with the surrounding defected region remaining undeformed. Such strain localization leads to reduced elongation and ductility loss. The primary defect clearing mechanisms are considered to be first a removal of the stacking fault in the loop by the stress field of glide dislocations and subsequent elimination of the loop by prismatic glide from the slip band [18].

However, the channel bands in deformed austenitic stainless steel are not devoid of microstructure. In addition to stacking faults and prototwins associated with the Shockley partials, there is debris in the form of jogs and stair-rod partials on Frank loops intersected by glide dislocations [18]. Such jogged partials are less mobile and remain in the bands, as observed in proton irradiated austenitic stainless steel [9]. These persistent loops impede dislocation motion continuously, sustaining the stress until a failure occurs. Despite the presence of these features, the bands can be imaged as defect-reduced channels by choosing an appropriate imaging condition.

As briefly mentioned already, in our previous work, it was found that when helium was implanted above 1 at.%, the helium-induced hardening exceeded that induced by displacement damage alone, using 3500 keV Fe^+ ions [1]. The hardening induced by helium tended to saturate near 10 at.% He level (7.5 dpa) to a value twice that produced by Fe-ion irradiation. Helium irradiation produced Frank loops as well as helium bubbles. Since helium bubbles are not removable defects, they remain in the channel bands even after many passes by dislocations. This is in contrast to the Frank loops, which are partially removed from the channel bands. Thus, helium bubbles not only impede the motion of dislocations in the matrix at early stages of deformation but also impede dislocation motion in the channel bands after channeling begins, thereby increasing both the yield strength and ultimate tensile strength. The additional hardening is thus attributable to these persistent helium bubbles. The microstructure depicted in Fig. 4 clearly confirms such a trend, although a quantitative measurement of such an effect could not be made from this particular microstructure.

5. Conclusions

Deformation microstructures were investigated for 316 LN austenitic stainless steel irradiated at 200°C to various doses with 360 keV He-ions and deformed to 10% strain at room temperature by a disk-bend method. The results showed that, with increasing dose, the mode of dislocation movement changed from planar glide with some cross-slip to a more restricted planar glide, due to pinning by helium bubbles and radiation-induced Frank loops. In particular, glide dislocations were spatially dissociated into distinct Shockley partials with increasing number and size of the Frank loops. Since widely separated partials cannot cross-slip easily, planar glide was enhanced.

Experimental evidence indicated that the presence of helium bubbles imposed an additional restriction on dislocation motion not only in the matrix but also in the channel bands, raising the hardness beyond the level achievable by displacement damage alone. However, since the effectiveness of helium pinning was observed at a helium level above 1 at.% (or when helium clusters assumed a well-defined bubble shape), it seems that helium bubbles have to reach a certain size to exert an appreciable barrier effect.

Acknowledgements

Research sponsored by the Division of Material Sciences and Engineering, Office of Basic Energy Sciences, US Department of Energy, under contract No. DE-AC05-00OR22725 with UT-Battelle, LLC.

References

[1] J.D. Hunn, E.H. Lee, T.S. Byun, L.K. Mansur, J. Nucl. Mater. 282 (2000) 131.
[2] I.G. Greenfield, H.G.F. Wilsdorf, J. Appl. Phys. 32 (1961) 827.
[3] U. Essmann, A. Seeger, Phys. Stat. Sol. 4 (1964) 177.
[4] J.L. Brimhall, Trans. Am. Inst. Min. Metall. Eng. 233 (1965) 1737.
[5] M.S. Wechsler, The Inhomogeneity of Plastic Deformation, American Society for Metals, Metals Park, OH, 1971, p. 18 (Chapter 2).
[6] J.L. Sharp, Philos. Mag. 16 (1972) 77.
[7] J.L. Sharp, Acta Metall. 22 (1974) 449.
[8] E.E. Bloom, Radiation Damage in Metals, American Society for Metals, Metals Park, OH, 1975, p. 295.
[9] M. Suzuki, A. Sato, T. Mori, Philos. Mag. 65 (1992) 1039.
[10] J.I. Cole, S.M. Bruemmer, J. Nucl. Mater. 225 (1995) 53.
[11] S.M. Bruemmer, J.I. Cole, R.D. Carter, G.S. Was, Mater. Res. Soc. Symp. Proc. 439 (1997) 437.
[12] J.L. Brimhall, J.I. Cole, J.S. Vetrano, S.M. Bruemmer, Mater. Res. Soc. Symp. Proc. 373 (1995) 177.

[13] S.G. Song, J.I. Cole, S.M. Bruemmer, Acta Mater. 45 (1997) 501.
[14] S.M. Bruemmer, J.I. Cole, R.D. Carter, G.S. Was, Mater. Res. Soc. Symp. Proc. 439 (1997) 437.
[15] M. Victoria, N. Baluc, C. Bailat, Y. Dai, M.I. Luppo, R. Schaublin, B.N. Singh, J. Nucl. Mater. 276 (2000) 114.
[16] N. Hashimoto, S.J. Zinkle, A.F. Rowcliffe, J.P. Robertson, S. Jitsukawa, J. Nucl. Mater. 283 (2001) 528.
[17] E.H. Lee, T.S. Byun, J.D. Hunn, M. Yoo, K. Farrell, L.K. Mansur, Acta Metall. (2001) submitted.
[18] E.H. Lee, M. Yoo, T.S. Byun, J.D. Hunn, K. Farrell, L.K. Mansur, Acta Metall. (2001) submitted.
[19] E.H. Lee, T.S. Byun, J.D. Hunn, N. Hashimoto, K. Farrell, J. Nucl. Mater. 281 (2000) 65.
[20] T.S. Byun, E.H. Lee, J.D. Hunn, K. Farrell, L.K. Mansur, J. Nucl. Mater. 294 (2001) 256.
[21] J.F. Ziegler, J.P. Biersack, U. Littmark, The Stopping and Range of Ions in Solids, Pergamon, New York, 1985.
[22] M.J. Norgett, M.T. Robinson, I.M. Torrens, Nucl. Eng. Des. 33 (1975) 50.
[23] E.H. Lee, Nucl. Instrum. and Meth. B 151 (1999) 29.
[24] D. Tabor, J. Inst. Met. 79 (1951) 1.
[25] T.S. Byun, E.H. Lee, J.D. Hunn, K. Farrell, L.K. Mansur, Small Specimen Test Techniques, vol. 4, ASTM STP 1418, American Society for Testing and Materials, West Conshohocken, PA, 2002, to be published.
[26] E.H. Lee, J.D. Hunn, T.S. Byun, L.K. Mansur, J. Nucl. Mater. 280 (2000) 18.
[27] D.J.H. Cockayne, I.L.F. Ray, M.J. Whelan, Philos. Mag. A 20 (1969) 1265.
[28] W.M. Stobbs, C.H. Sworn, Philos. Mag. 24 (1971) 1365.
[29] V. Gerold, H.P. Karnthaler, Acta. Metall. 37 (1989) 2177.
[30] M.S. Wechsler, The Inhomogeneity of Plastic Deformation, American Society for Metals, Metals Park, OH, 1971, p. 18 (Chapter 2).
[31] J.V. Sharp, Philos. Mag. 16 (1967) 77.
[32] L.M. Lowe, Radiat. Eff. 23 (1974) 181.
[33] A. Okada, R. Kanao, T. Yoshiie, S. Kojima, Mater. Trans. JIM 30 (1989) 265.
[34] E.H. Lee, N.H. Packan, M.B. Lewis, L.K. Mansur, Nucl. Instrum. and Meth. B 16 (1986) 251.
[35] J.E. Pawel, A.F. Rowcliffe, D.J. Alexander, M.L. Grossbeck, K. Shiba, J. Nucl. Mater. 233–237 (1996) 202.
[36] J. Chen, Y. Dai, F. Carsughi, W.F. Sommer, G.S. Bauer, H. Ullmaier, J. Nucl. Mater. 275 (1999) 115.